Inorganic Chemistry

Article

Coordination "Oligomers" in Self-Assembly Reactions of Some "Tritopic" Picolinic Dihydrazone Ligands—Mononuclear, Dinuclear, Hexanuclear, Heptanuclear, and Nonanuclear Examples

Virginie Niel,[†] Victoria A. Milway,[†] Louise N. Dawe,[†] Hilde Grove,[†] Santokh S. Tandon,[§] Tareque S. M. Abedin,[†] Timothy L. Kelly,[†] Elinor C. Spencer,[‡] Judith A. K. Howard,[‡] Julie L. Collins,[†] David O. Miller,[†] and Laurence K. Thompson*,[†]

Department of Chemistry, Memorial University, St. John's, Newfoundland A1B 3X7, Canada, University of Durham, South Road, Durham DH1 3LE, U.K., and Kent State University, Salem Campus, Salem, Ohio 44460

"Tritopic" picolinic dihydrazone ligands with tridentate coordination pockets are designed to produce homoleptic [3 × 3] nonanuclear square grid complexes on reaction with transition-metal salts, and many structurally documented examples have been obtained with Mn(II), Cu(II), and Zn(II) ions. However, other oligomeric complexes with smaller nuclearities have also been discovered and identified structurally in some reactions involving Fe(II), Co(II), Ni(II), and Cu(II), with certain tritopic ligands. This illustrates the dynamic nature of the metal–ligand interaction and the conformationally flexible nature of the ligands and points to the possible involvement of some of these species as intermediates in the [3 × 3] grid formation process. Examples of mononuclear, dinuclear, hexanuclear, heptanuclear, and nonanuclear species involving Fe(II), Co(II), Ni(II), and Cu(II) salts with a series of potentially heptadentate picolinic dihydrazone ligands with pyrazine, pyrimidine, and pyridine end groups are described in the present study. Iron and cobalt complexation reactions are complicated by redox processes, which lead to mixed-oxidation-state Co(II)/Co(III) systems when starting with Co(II) salts, and reduction of Fe(III) to Fe(II) when starting with Fe(III). Magnetic exchange within the polynuclear structural frameworks is discussed and related to the structural features.

Introduction

Self-assembly methods for the synthesis of "pre-organized" polynuclear structural arrays are predicated on the strategic placement of appropriate design elements in a ligand and the assumption that the coordination algorithm of the metal ion interprets this programmed coordination information appropriately. This has had a significant measure of success with linear "polytopic" ligands based on pyridazine bridging subunits, which have produced molecular [2 × 2] Cu(I)4[1] (ditopic ligand) and [3 × 3] Ag(I)9[2,3] (tritopic ligand) grids involving four-coordinate metal centers, by a strict self-assembly process. Pb16 [4 × 4] grids, involving six-coordinate metal centers, have also been produced with extended tetratopic pyrimidine-based ligands.[4,5] However, with these metal ions, crystal field effects are not part of the overall thermodynamic energy balance, and the self-assembly process depends largely on the organizing influence of the ligand, the donor arrangements within the coordination pockets, and to a lesser extent, on the stereochemical preferences of the metal.

[2 × 2] heteroleptic, tetrametallic grids involving six-coordinate transition-metal ions have been produced with ditopic ligands based on 2-picolinic hydrazone subunits, where hydrazone oxygen atoms bridge the metal centers and

* To whom correspondence should be addressed. E-mail: lthomp@mun.ca.
† Memorial University.
‡ University of Durham.
§ Kent State University.
(1) Youinou, M-T.; Rahmouni, N.; Fischer, J.; Osborn, J. A. *Angew. Chem., Int. Ed.* **1992**, *31*, 733.
(2) Baxter, P. N. W.; Lehn, J-M.; Fischer, J.; Youinou, M-T. *Angew. Chem., Int. Ed.* **1994**, *33*, 2284.
(3) Baxter, P. N. W.; Lehn, J-M.; Kneisel, B. O.; Fenske, D. *Angew. Chem., Int. Ed.* **1997**, *36*, 1978.
(4) Garcia, A. M.; Romero-Salguero, F. J.; Bassani, D. M.; Lehn, J-M.; Baum, G.; Fenske, D. *Chem.—Eur. J.* **1999**, *5*, 1803.
(5) Onions, S. T; Franklin, A. M.; Horton, P. N.; Hursthouse, M. B.; Matthews, C. J. *Chem. Commun.* **2003**, 2864.

Coordination Oligomers in Self-Assembly Reactions

Chart 1. Tritopic Pyridine Dihydazone Ligands
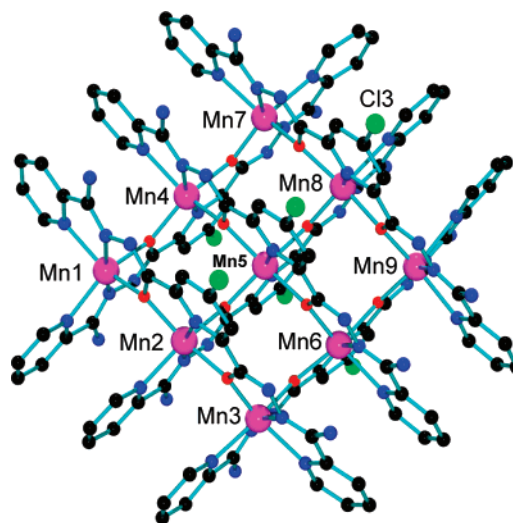

2noap
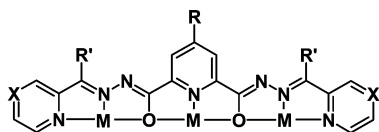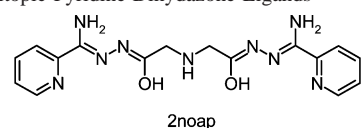
2poap (R=H, R'=NH$_2$, X=CH),Cl2poap (R=Cl, R'=NH$_2$,
X=CH), 2popp (R=H, R'=Ph, X=CH), Cl2popp (R=Cl,
R'=Ph, X=CH), Cl2pomp (R=Cl, R'=Me, X=CH), 2pzoap
(R=H, R'=NH$_2$, X=N), Cl2poapz (R=Cl, R'=NH$_2$, X=N),
SEt2poap (R=SEt, R'=NH$_2$, X=CH)

2pmoap

L1
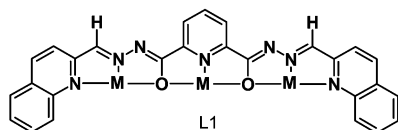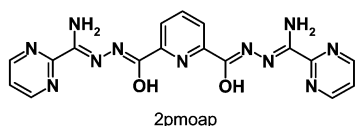
Scheme 1. Self-Assembly Scheme for M$_9$ and M$_8$
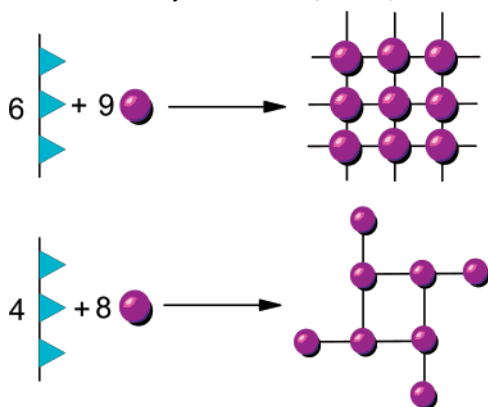
can lead to intramolecular spin exchange.[6,7] Related tritopic ligands, such as 2poap and its derivatives (Chart 1), so far have formed homoleptic [3 × 3] nonanuclear grids (Scheme 1) as the dominant products,[8−16] although in a few cases complexes of lower nuclearity have been produced. The

Figure 1. POVRAY structural representation of the cation in [Mn$_9$-(Cl2poap)$_6$](ClO$_4$)$_6$.

complex [Mn$_9$(Cl2poap)$_6$](ClO$_4$)$_6$ (Scheme 1 and Figure 1) is a typical nonanuclear example,[14] which highlights the complementary fit of the six ligands arranged in two parallel groups of three above and below the [Mn$_9$-(μ-O)$_{12}$] core. The syn ligand conformation brings the two hydrazone oxygen bridges and the nitrogen donor atoms into the correct alignment for efficient [3 × 3] grid self-assembly. Octa-nuclear heteroleptic [Cu$_8$L$_4$] "pinwheel" clusters (Scheme 1) form with the ligand in the same syn conformation when anion and solvent competition appear to prevent [3 × 3] grid formation.[17,18]

A pentanuclear [Fe(III)$_5$L$_6$] "remote" symmetric square grid forms with Cl2poap,[14] in which metal ions occupy just the corner and center positions of a typical [3 × 3] grid arrangement of ligands, with the other sites being empty. A dinuclear spiral complex, [Ni$_2$(2pzoap)$_3$F](BF$_4$)$_3$·8.5H$_2$O,[19a,b] forms in preference to a grid, in which a central cavity is occupied by an adventitious fluoride ion derived from the hydrolysis of BF$_4^-$. The dinuclear complex [Ni$_2$(2poap)$_2$(H$_2$O)$_2$](NO$_3$)$_4$ forms as one product in the reaction of Ni(NO$_3$)$_2$ with 2poap.[20] This type of ligand can also produce trinuclear complexes, e.g.,

(6) Thompson, L. K.; Matthews, C. J.; Zhao, L.; Xu, Z.; Miller. D. O.; Wilson. C.; Leech, M. A.; Howard, J. A. K.; Heath, S. L.; Whittaker, A. G.; Winpenny, R. E. P. *J. Solid State Chem.* **2001**, *159*, 308.
(7) Matthews, C. J.; Avery, K.; Xu, Z.; Thompson, L. K.; Zhao, L.; Miller, D. O.; Biradha, K.; Poirier, K.; Zaworotko, M. J.; Wilson, C.; Goeta, A. E.; Howard, J. A. K. *Inorg. Chem.* **1999**, *38*, 5266.
(8) Zhao, L.; Matthews, C. J.; Thompson, L. K.; Heath, S. L. *Chem. Commun.* **2000**, 265.
(9) Zhao, L.; Xu, Z.; Thompson, L. K.; Heath, S. L.; Miller, D. O.; Ohba, M. *Angew. Chem., Int. Ed.* **2000**, *39*, 3114.
(10) Waldmann, O.; Koch, R.; Schromm, S.; Müller, P.; Zhao, L.; Thompson, L. K. *Chem. Phys. Lett.* **2000**, *332*, 73.
(11) Waldmann, O.; Zhao, L.; Thompson, L. K. *Phys. Rev. Lett.* **2002**, *88*, 066401−1−4.
(12) Zhao, L.; Xu, Z.; Thompson, L. K.; Miller, D. O. *Polyhedron* **2001**, *20*, 1359.

(13) Dawe, L. N.; Abedin, T. S. M.; Kelly, T. L.; Thompson, L. K.; Miller, D. O.; Zhao, L.; Wilson, C.; Leech, M. A.; Howard, J. A. K. *J. Mater. Chem.* **2006**, *16*, 2645.
(14) Thompson, L. K.; Zhao, L.; Xu, Z.; Miller, D. O.; Reiff, W. M. *Inorg. Chem.* **2003**, *42*, 128.
(15) (a) Zhao, L.; Xu, Z.; Grove, H.; Milway, V. A.; Dawe, L. N.; Abedin, T. S. M.; Thompson, L. K.; Kelly, T. L.; Harvey, R. G.; Miller, D. O.; Weeks, L.; Shapter, J. G.; Pope, K. J. *Inorg. Chem.* **2004**, *43*, 3812. (b) Milway, V. A.; Thompson, L. K.; Miller, D. O. *Chem. Commun.* **2004**, 1790.
(16) Milway, V. A.; Abedin, T. S. M.; Niel, V.; Kelly. T. L.; Dawe, L. N.; Dey, S. K.; Thomson. D. W.; Miller, D. O.; Alam, M. S.; Müller, P.; Thompson, L. K. *Dalton Trans.* **2006**, 2835.
(17) Xu, Z.; Thompson, L. K.; Miller, D. O. *Chem. Commun.* **2001**, 1170.
(18) Milway, V. A.; Niel, V.; Abedin, T. S. M.; Xu, Z.; Thompson, L. K.; Grove, H.; Miller, D. O.; Parsons, S. R. *Inorg. Chem.* **2004**, *43*, 1874.
(19) (a) Thompson, L. K.; Matthews, C. J.; Zhao, L.; Wilson, C.; Leech, M. A.; Howard, J. A. K. *J. Chem. Soc., Dalton Trans.* **2001**, 2258. (b) Wamser, C. A. *J. Am. Chem. Soc.* **1948**, *70*, 1209.
(20) Zhao, L.; Niel, V.; Thompson, L. K.; Xu, Z.; Milway, V. A.; Harvey, R. G.; Miller, D. O.; Wilson, C.; Leech, M.; Howard J. A. K.; Heath, S. L. *Dalton Trans.* **2004**, 1446.

[Cu₃(2poap-2H)(CH₃COO)₄]·3H₂O,[21] in the presence of carboxylate ligands, which coordinate and serve to impede the formation of a nonanuclear grid. The more flexible tritopic ligand 2noap (Chart 1) shows no tendency to form [3 × 3] grids in studies carried out so far, but has instead formed mainly trinuclear complexes.[22]

The specific mechanism for [3 × 3] grid assembly is difficult to determine, but seems unlikely to occur as a concerted single-step process involving the assembly of six ligands and nine metals at the same time. On the basis of the various examples of polynuclear complexes which are known with ligands in this class, it seems more likely that simpler mononuclear and polynuclear precursor fragments form first and then assemble into the grid, perhaps involving several assembly steps. In this context, a variety of "oligomeric" species may be expected, depending on the ligand geometric conformation, the particular metal ion involved, and other conditions, e.g., the solvent used, the temperature, the pH of the synthetic medium, and the nature of the counterion used. Also, depending on the assembly route, some steps may end up being "terminal" as a result of the formation of species where, e.g., the incorrect ligand conformation has been chosen.

In this report, a number of new oligomeric complexes are reported, which have been identified by X-ray crystallography, and include mononuclear, dinuclear, hexanuclear, heptanuclear, and nonanuclear examples. Some of these could be components in grid assembly or further examples in a potentially vast library of different complexes which could form as a result of the dynamic nature of the metal−ligand interactions, the flexibility of the ligands, and their different possible bonding conformations. Structural and magnetic properties are discussed.

Experimental Section

Physical Measurements. Infrared spectra were recorded as Nujol mulls using a Mattson Polaris FT-IR instrument, and UV−vis spectra were obtained as Nujol mulls or in solution using a Cary 5E spectrometer. Microanalyses were carried out by Canadian Microanalytical Service, Delta, Canada. Variable-temperature magnetic data (2−300 K) were obtained using a Quantum Design MPMS5S SQUID magnetometer with a field strength of 0.1 T. Background corrections for the sample holder assembly and diamagnetic components of the complexes were applied.

Synthesis of Complexes. In some cases, there is a difference between the most reasonable formula based on the elemental analysis (analytical formula) and that obtained from X-ray crystallography. For consistency, the analytical formulas will be used.

[Fe(Cl2poapz)(H₂O)₂](ClO₄)·1.5H₂O (1). Cl2poapz[14] (0.10 g, 0.23 mmol) dissolved in methanol (6 mL) was added to a solution of Fe(ClO₄)₃·6H₂O (0.16 g, 0.46 mmol) in methanol (5 mL), resulting in the formation of a green solution. A small quantity (yield 0.015 g, 10%) of orange-brown crystals was obtained on prolonged standing at room temperature for several weeks. Elemental Anal. Calcd (air-dried sample) for (C₁₇H₁₂N₁₁O₂Cl)Fe-

(ClO₄)(H₂O)₃.₅: C, 31.12; H, 2.92; N, 23.48. Found: C, 30.99; H, 2.25; N, 23.25.

[Cu(SEt2poap-H)(ClO₄)](ClO₄)(CH₃CN) (2). In an attempt to produce a mixed-metal [3 × 3] grid, Mn(ClO₄)₂·6H₂O (0.11 g, 0.30 mmol) and Cu(ClO₄)₂·6H₂O (0.21 g, 0.57 mmol) were dissolved in methanol (10 mL). SEt2poap[16] (0.20 g, 0.43 mmol) was added, resulting in the formation of a yellow-green solid. Acetonitrile (10 mL) was added, and the precipitate was dissolved, forming a clear yellow-brown solution. Methanol (20 mL) was added, and the mixture was heated at ∼60 °C for 2 h, with the formation of a green-yellow microcrystalline solid (yield 0.18 g, 54%). The solid product was recrystallized from an acetonitrile/methanol mixture (30 mL, 6:1), resulting in brown crystals suitable for X-ray structural determination. Elemental Anal. Calcd for (C₂₁H₂₁N₉O₂S)Cu-(ClO₄)₂(CH₃CN): C, 36.02; H, 3.15; N, 18.26. Found: C, 36.00; H, 3.18: N, 18.26.

[Ni₂(2pmoap)₂(CH₃CN)₂](ClO₄)₄·4H₂O (3). 2pmoap[13] (0.15 g, 0.37 mmol) was added to a solution of Ni(ClO₄)₂·6H₂O (0.24 g, 0.67 mmol) in 20 mL of 50:50 CH₃OH/CH₃CN. Three drops of Et₃N was added to the resulting clear, olive-green solution. The solution turned brown and was stirred with gentle heating at ∼40 °C for 1 h and then filtered. After 4 days, the filtrate was layered with diethyl ether, producing green prismatic crystals after 3 weeks, suitable for X-ray analysis (yield 0.12 g, 45%). Elemental Anal. Calcd on the bulk air-dried sample for (C₁₇H₁₅N₁₁O₂)₂Ni₂(ClO₄)₄(H₂O)₄(CH₃CN)₂: C, 28.57; H, 2.78; N, 21.04. Found: C, 28.40; H, 2.94; N, 21.07.

[Ni₂(Cl2poap)₃F](BF₄)₃·5H₂O (4) and [Ni₆(Cl2poap-2H)₅]-(BF₄)₄[Ni(H₂O)₆]·20H₂O (8). Cl2poap[14] (0.22 g, 0.50 mmol) was added to a solution of Ni(BF₄)₂·6H₂O (0.37 g, 1.0 mmol) in methanol/acetronitrile (15/15 mL). Et₃N (1 drop) was added, and the mixture was heated until the ligand dissolved. The resulting green solution was filtered and allowed to evaporate slowly at room temperature. A mixture of green and brown crystals formed after several weeks, which were then separated by hand to obtain samples for structural, magnetic, and elemental analysis. The green crystalline material was estimated at ∼20% of the bulk sample. Elemental Anal. Calcd for (C₁₉H₁₆N₉O₂Cl)₃Ni₂F(BF₄)₃(H₂O)₅ (4) (brown sample dried in air): C, 36.92; H, 3.48; N, 20.39. Found: C, 36.77; H, 2.75: N, 20.25. Elemental Anal. Calcd for (C₁₉H₁₄N₉O₂Cl)₅Ni₇-(BF₄)₄(H₂O)₂₆ (8) (green sample exposed to air): C, 33.50; H, 3.61; N, 18.51. Found: C, 33.44; H, 2.52: N, 18.44.

[Fe₂(2popp)₃F](PF₆)₃·2H₂O (5). A solution of Fe(ClO₄)₃·6H₂O (0.050 g, 0.14 mmol) dissolved in methanol (20 mL) was added to a solution of 2popp[15] (0.050 g, 0.10 mmol) in chloroform (15 mL). NH₄PF₆ (0.070 g, 0.40 mmol) dissolved in 15 mL of methanol was then added. The resulting pink solution was allowed to stand at room temperature. Dark purple-black needle-shaped crystals of **5** appeared after several days (yield 0.065 g, 30%). Elemental Anal. Calcd for (C₃₁H₂₃N₇O₂)₃Fe₂(PF₆)₃F(H₂O)₂: C, 51.26; H, 3.35; N, 13.50. Found: C, 50.79; H, 3.31; N, 13.52.

[Fe₂(2popp)₃Cl](ClO₄)₃·6H₂O (6). Purple-colored crystals of **6**, suitable for a structural determination, were obtained using slow diffusion in an "H" tube, in which 2popp[15] (0.10 g, 0.19 mmol) in solution in chloroform was introduced in one side and Fe(ClO₄)₃·6H₂O (0.10 g, 0.28 mmol) dissolved in methanol was placed in the other. The H tube solution volume was completed with methanol. (Yield 0.015 g, 11%). Elemental Anal. Calcd for (C₃₁H₂₃N₇O₂)₃Fe₂(ClO₄)₃Cl(H₂O)₆: C, 53.01; H, 3.90; N, 13.81. Found: C, 52.60; H, 3.43; N, 13.82.

[Ni₆(SEt2poap)₅](CF₃SO₃)₇·14H₂O (7). Ni(CF₃SO₃)₂(aq) (30 mL (0.08 g·mL⁻¹), 6.7 mmol) was diluted with methanol, and SEt2poap[16] (1.04 g, 2.2 mmol) was added. The ligand dissolved,

(21) Zhao, L.; Thompson, L. K.; Xu, Z.; Miller, D. O.; Stirling, D. R. *J. Chem. Soc., Dalton Trans.* **2001**, 1706.
(22) Milway, V. A.; Zhao, L.; Abedin, T. S. M.; Thompson, L. K.; Xu, Z. *Polyhedron* **2003**, *22*, 1271.

forming a clear green-brown solution, which was heated for 8 h at ~60 °C, then filtered and left to stand. Green-brown crystals (yield 0.35 g, 20%) suitable for X-ray crystallography formed after several days. Elemental Anal. Calcd for $[(C_{21}H_{21}N_9O_2S)_2(C_{21}H_{20}N_9O_2S)$-$(C_{21}H_{19}N_9O_2S)_2Ni_6](CF_3SO_3)_7(H_2O)_{14}$: C, 33.97; H, 3.26; N, 15.92. Found: C, 33.96; H, 2.85; N, 15.95.

$[Co_7(2poap-2H)_5](ClO_4)_8 \cdot 5CH_3CN \cdot 11H_2O$ (9). 2poap[8] (0.28 g, 0.69 mmol) was added to a warm solution of $Co(ClO_4)_2 \cdot 6H_2O$ (0.57 g, 1.6 mmol) in $CH_3CN/MeOH/H_2O$ (20/10/10 mL) with stirring. The ligand dissolved forming a deep-red-colored solution, which darkened on standing in air. A brown microcrystalline solid formed on prolonged standing for several weeks (yield 0.33 g, 70%). A portion of the bulk sample was recrystallized from $MeOH/CH_3CN$ to give a small quantity of brown rectangular-shaped crystals, suitable for structural analysis and magnetic study. Elemental Anal. Calcd on bulk sample for $(C_{19}H_{15}N_9O_2)_5Co_7(ClO_4)_8(CH_3CN)_5$-$(H_2O)_{11}$: C, 34.85; H, 3.12; N, 19.35. Found: C, 35.13; H, 2.90; N, 19.27.

$[Ni_9(Cl2popp)_5(OH)_2(CH_3CN)_2(H_2O)_3](ClO_4)_6 \cdot 19H_2O$ (10). Cl2popp[15a,b] (0.10 g, 0.20 mmol) was added to a solution of Ni-$(ClO_4)_2 \cdot 6H_2O$ (0.24 g, 0.70 mmol) in 30 mL of acetonitrile, forming a clear-green solution, which was heated to ~60 °C for 1 h. A portion of 10 mL of absolute ethanol was added to the resulting brown solution, which was then allowed to stand at room temperature, producing brown crystals over several days (yield 0.060 g, 35%), which were suitable for structural study. Vis−NIR (acetonitrile): $\lambda_1 = 1180$ nm, $\lambda_2 = 844$ nm. Elemental Anal. Calcd for $(C_{31}H_{20}N_7O_2Cl)_5Ni_9(OH)_2(CH_3CN)_2(ClO_4)_6(H_2O)_{22}$: C, 43.18; H, 3.46; N, 11.70. Found: C, 43.20; H, 2.88; N, 11.53.

Crystallographic Data and Refinement of the Structures. The diffraction intensities of an amber block-shaped crystal of **1** of dimensions $0.02 \times 0.02 \times 0.03$ mm were collected with graphite-monochromatized Mo Kα X-radiation $\lambda = 0.71073$ Å (Bede Microsource) using a Bruker Proteum M diffractometer. The crystal was cooled to 120(1) K using an Oxford Cryosystems Cryostream.[23] Data were collected to a maximum 2θ value of 52.0°. The data were corrected for Lorentz and polarization effects. All data processing was carried out using the *SAINT*[24] and *XPREP*[25] software packages. Absorption corrections were applied using *SADABS*.[26] The structures were solved by direct methods and refined on F^2 using full-matrix least-squares methods within the *SHELXTL*[27] suite. Neutral atom scattering factors[28] and anomalous-dispersion terms[29,30] were taken from the usual sources. All non-hydrogen atoms were refined anisotropically. Hydrogen atom positions were calculated geometrically or located in the difference map. Geometrically included hydrogen atoms were treated with a riding model, with isotropic thermal parameters set 20% greater than their bonded partners. The model contains two water molecules, whose associated protons have not been included in the model. One perchlorate

oxygen atom is disordered over two sites. Abbreviated crystal data are given in Table 1.

The diffraction intensities of a red-black prismatic crystal of **5** of dimensions $0.53 \times 0.16 \times 0.13$ mm were collected with graphite-monochromatized Mo Kα X-radiation using a Bruker P4/CCD diffractometer at 193(2) K to a maximum 2θ value of 52.8°. The data were corrected for Lorentz and polarization effects. The structure was solved by direct methods[31] and expanded using Fourier techniques.[32] All atoms except those of hydrogen were refined anisotropically. Hydrogen atoms were included in calculated or difference map positions with isotropic thermal parameters set to 20% greater than their bonded partners at the time of their inclusion and were not refined. Neutral atom scattering factors[28] and anomalous-dispersion terms[29,30] were taken from the usual sources. All other calculations were performed with the *teXsan*[33] crystallographic software package. Abbreviated crystal data are given in Table 1. Complexes **6** (brown plate $0.40 \times 0.31 \times 0.11$ mm) and **9** (brown prism $0.78 \times 0.49 \times 0.44$ mm) were treated in a similar manner, and crystal data are given in Table 1. In **6**, five hydrazone hydrogen atoms were found in difference maps and optimized by positional refinement, but were fixed for the final round of refinement. A disordered chloroform molecule and a disordered perchlorate were found in the lattice. The disordered perchlorate anion was refined isotropically and held with fixed atomic positions and thermal parameters in the final round of least squares in order to achieve convergence. The presence of an electron density trough of 4.0 e·Å^{-3} is attributed to this disorder.

The diffraction intensities of a brown prismatic crystal of **2** of dimensions $0.25 \times 0.20 \times 0.15$ mm were collected with graphite-monochromatized Mo Kα X-radiation using a Rigaku AFC8 Saturn CCD diffractometer at 153(2) K to a maximum 2θ value of 61.4°. The data were corrected for Lorentz and polarization effects. The structure was solved by direct methods[31] and expanded using Fourier techniques. Neutral atom scattering factors were taken from Cromer and Waber.[28] Anomalous dispersion effects were included in *Fcalc*;[29] the values for $\Delta f'$ and $\Delta f''$ were those of Creagh and McAuley.[30] The values for the mass attenuation coefficients are those of Creagh and Hubbell.[34] All calculations were performed using the *CrystalStructure*[35,36] crystallographic software package. Hydrogen atoms were included in calculated or difference map positions with isotropic parameters set 20% greater than those of their bonding partners. Three methyl protons on acetonitrile are missing from the model, and the acetonitrile group is disordered. All hydrogen atoms were held in riding positions. Significant residual electron density peaks ($+3.14$ e$^-$/Å^3, -3.69 e$^-$/Å^3) were located close to the copper center. Abbreviated crystal data are given in Table 1. Data collection and solution refinement for **3** (green prism $0.22 \times 0.20 \times 0.17$ mm), **4** (brown prism $0.44 \times 0.43 \times 0.41$ mm), **7** (green-brown prism, $0.29 \times 0.20 \times 0.094$ mm), and **8** (green prism $0.44 \times 0.45 \times 0.34$ mm) were carried out in a similar

(23) Cosier, J.; Glazer, A. M. *J. Appl. Crystallogr.* **1986**, *19*, 105.

(24) Sheldrick, G. M. *SAINTPLUS*, version 6.02; Bruker AXS: Madison, WI, 1997.

(25) Sheldrick, G. M. *SHELXS-97* and *SHELXL-97*, *Programs for the Refinement of Crystal Structures*; University of Göttingen: Göttingen, Germany, 1998.

(26) Sheldrick, G. M. *SADABS. Program for Absorption Correction*; University of Göttingen: Göttingen, Germany, 1998.

(27) *SHELXTL,* version 5.1; Bruker AXS: Madison, WI.

(28) Cromer, D. T.; Waber, J. T. *International Tables for X-ray Crystallography*; The Kynoch Press: Birmingham, England, 1974; Vol. IV, table 2.2 A.

(29) Ibers, J. A.; Hamilton, W. C. *Acta Crystallogr.* **1964**, *17*, 781.

(30) Creagh, D. C.; McAuley, W. J. *International Tables for Crystallography*; Wilson, A. J. C., Ed.; Kluwer Academic Publishers: Boston, 1992; Vol. C, Table 4.2.6.8, pp 219−222.

(31) Sheldrick, G. M. *SHELX97*; University of Göttingen: Göttingen, Germany, 1997.

(32) Beurskens, P. T.; Admiraal, G.; Beurskens, G.; Bosman, W. P.; de Gelder, R.; Israel, R.; Smits, J. M. M. *DIRDIF99*: *The DIRDIF-94 Program System*; Technical Report of the Crystallography Laboratory, University of Nijmegen: Nijmegen, The Netherlands, 1999.

(33) *teXsan for Windows*: *Crystal Structure Analysis Package*; Molecular Structure Corporation, 1997.

(34) Creagh, D. C.; Hubbell, J. H. *International Tables for Crystallography*; Wilson, A. J. C., Ed.; Kluwer Academic Publishers: Boston, 1992; Vol. C, Table 4.2.4.3, pp 200−206.

(35) *CrystalStructure 3.7.0*: *Crystal Structure Analysis Package*; Rigaku and Rigaku/MSC: The Woodlands, TX, 2000−2005.

(36) Watkin, D. J.; Prout, C. K.; Carruthers, J. R.; Betteridge, P. W. *CRYSTALS Issue 10*; Chemical Crystallography Laboratory, Oxford, U.K., 1996.

Table 1. Summary of Crystallographic Data for **1−9**

compound	1	2	3	4
empirical formula	$C_{17}H_{12}Cl_2FeN_{11}O_{11}$	$C_{23}H_{24}Cl_2CuN_{10}O_{10}S$	$C_{44}H_{61}Cl_4N_{27}Ni_2O_{26.5}$	$C_{62}H_{71}B_3Cl_3F_{13}N_{29}Ni_2O_{13.5}$
M	675.14	767.02	1651.34	1941.6
cryst syst	monoclinic	triclinic	triclinic	triclinic
space group	$P2_1/c$ (No. 14)	$P\bar{1}$ (No. 2)	$P\bar{1}$ (No. 2)	$P\bar{1}$ (No. 2)
a/Å	17.183(5)	8.776(2)	12.2347(11)	13.4278(19)
b/Å	16.435(4)	12.763(4)	13.4388(16)	17.609(3)
c/Å	9.195(2)	13.574(4)	13.5736(3)	17.642(3)
α/deg		99.273(8)	61.16(2)	96.742(3)
β/deg	98.942(6)	95.011(8)	67.15(2)	94.035(3)
γ/deg		93.427(10)	76.63(3)	98.330(3)
V/Å^3	2565.2(11)	1490.5(8)	1798.8(3)	4082.7(11)
ρ_{calcd}/g cm^{-3}	1.748	1.709	1.524	1.579
T/K	120(2)	153(2)	153(2)	153(2)
Z	4	2	1	2
μ/cm^{-1}	8.77	10.555	7.662	6.68
reflections collected[a]				
total, unique, R_{int},	15 970, 5037,0.1499	16 456, 7850, 0.019	20 233, 9612, 0.022	39 927, 21323, 0.020
obs ($I > 2.00\sigma(I)$)	2752	7850	9612	21 323
final R_1, R_2	0.0694, 0.1403	0.1010, 0.1139	0.067, 0.2017	0.0577, 0.1425

compound	5	6	7	8	9
empirical formula	$C_{93}H_{67}N_{21}O_{6.5}$-$F_{19}P_3Fe_2$	$C_{94}H_{75}N_{21}O_{20.5}$-$Cl_7Fe_2$	$C_{113}H_{149}F_{21}N_{45}$-$Ni_6O_{54.5}S_{12}$	$C_{100}H_{115.5}B_4Cl_5F_{16}$-$N_{47.5}Ni_7O_{28.5}$	$C_{107}H_{115}N_{51}O_{53}$-$Co_7Cl_8$
M	2148.27	2186.62	4145.58	3380.36	3659.55
cryst syst	monoclinic	triclinic	triclinic	monoclinic	triclinic
space group	$P2_1/c$ (No. 14)	$P\bar{1}$ (No. 2)	$P\bar{1}$ (No. 2)	$P2_1/n$ (No. 14)	$P\bar{1}$ (No. 2)
a/Å	19.669(1)	13.697(1)	18.6174(14)	24.0969(19)	15.274(1)
b/Å	16.960(1)	13.707(1)	19.2391(15)	20.2311(16)	19.268(1)
c/Å	29.728(2)	28.756(2)	26.272(2)	30.161(3)	29.766(2)
α/deg		96.513(2)	79.147(7)		91.840(2)
β/deg	103.345(1)	93.283(2)	74.629(6)	95.112(2)	99.088(1)
γ/deg		116.913(1)	77.008(7)		97.501(1)
V/Å^3	9649(1)	4746.8(6)	8758.0(12)	14645(2)	8564(1)
ρ_{calcd}/g cm^{-3}	1.479	1.530	1.572	1.533	1.419
T/K	193(2)	193(2)	153(2)	153(2)	193(2)
Z	4	2	2	4	2
μ/cm^{-1}	4.52	5.87	8.89	10.74	7.72
rflns collected[a]					
total, unique, R_{int},	58 834, 19 751, 0.063	23 790, 18 363, 0.038	99 114, 47 243, 0.052	139 707, 33 393, 0.0506	50822, 34243, 0.024
obs ($I > 2.00\sigma(I)$)	12 398	18 363	47 243	33 393	23 846
final R_1, R_2	0.078, 0.246	0.1037, 0.3322	0.1086, 0.2828	0.1045, 0.3069	0.088,0.301

[a] $R_1 = \Sigma[|F_o| - |F_c|]/\Sigma|F_o|$, $R_2 = [\Sigma[w(|F_o|^2 - |F_c|^2)^2]/\Sigma[w(|F_o|^2)^2]]^{1/2}$, $R = \Sigma||F_o| - |F_c||/\Sigma|F_o|$, $R_2 = [\Sigma w(|F_o| - |F_c|)^2/\Sigma wF_o^2]^{1/2}$.

manner. For **3**, the symmetry-expanded model contains a total of 6.5 partially occupied lattice solvent water molecules. Their associated hydrogen atoms were omitted from the model. Abbreviated crystal data are given in Table 1.
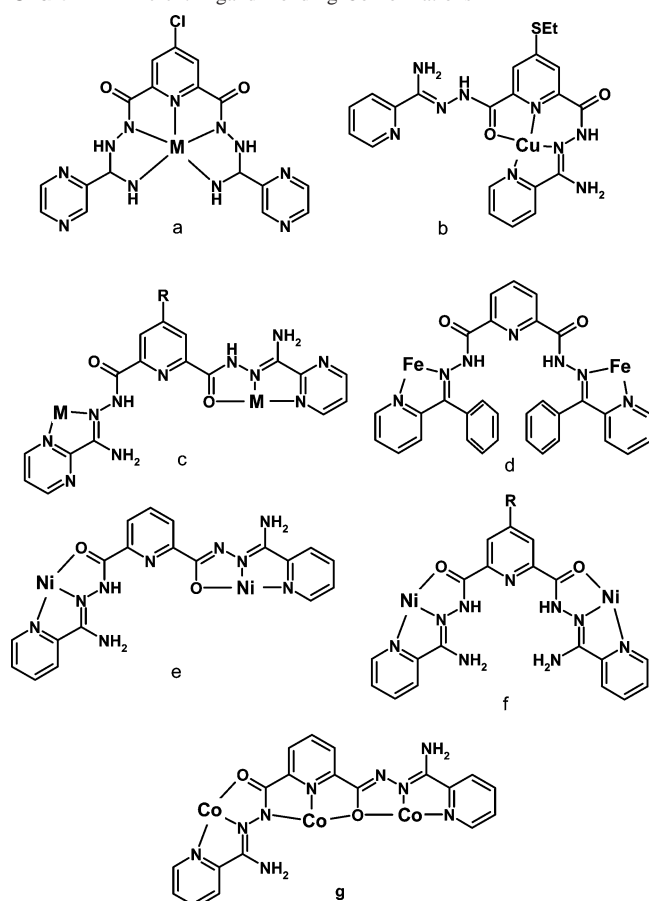
Results and Discussion

Structures. [Fe(Cl2poapz)(H₂O)₂](ClO₄)·1.5H₂O (1). The structure of the mononuclear cation in **1** is shown in Figure 2, and relevant bond distances and angles are listed in Table 2. The Fe(III) ion has a pentagonal-bipyramidal stereochemistry and binds to a single pentadentate (N₅) (Chart 2a). Cl2poapz ligand, which adopts an unusual chelating conformation, with nitrogen atoms from the central pyridine, two diazine groups, and, surprisingly, two amidrazone type NH₂ groups, both of which appear to be deprotonated, bonded in the pentagonal metal plane. N−Fe−N angles within the plane fall in the range 68.4−80.5 °, with an average of 72.0(2)°. The solid angle for these five bonds of 360.2° indicates the flat nature of the pentagonal plane. Single protons are located on N(3), N(4), N(8), and N(9), leading to a −2 charge on the ligand. In accordance, C−O (O1 and O2) bond distances are short (1.258(6) and 1.271-

(6) Å), indicating significant double-bond character, and C−N bonds to N(4) and N(9) (1.302(7) and 1.279(6) Å, respectively) are also short, indicating significant C=N double-bond character. Establishing the exact sites of deprotonation in ligands of this type is usually difficult, because of significant charge delocalization within the O−C−N−N−C−N open chain framework. The single perchlorate ion observed in the lattice balances the charge and is hydrogen bonded to the two protons bound to N(4) and N(9).

Fe donor distances fall in the range of 2.034(4)−2.250(5) Å, with the shortest contacts to the axial water molecules (O(3) and O(4)). The longer in-plane metal−ligand distances are perhaps not typical of Fe(III), but the charged state of the metal is not in doubt (vide infra). This situation likely results from the strain produced when the ligand is forced to bend around the single metal ion and form the five in-plane Fe−N bonds and the close-to-planar arrangement of adjacent five-membered chelate rings. The planarity also extends to include the external, uncoordinated pyrazine rings. It is of interest to note that external N₂O donor "pockets" are created as a result of the way in which the ligand is bent
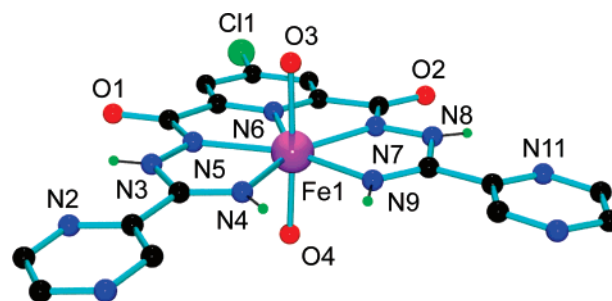
Chart 2. Different Ligand Bonding Conformations

Figure 2. POVRAY structural representation of the cation in **1**.

Table 2. Bond Lengths (Å) and Angles (deg) for **1**

Fe1−O4	2.034(4)	O4−Fe1−O3	176.07(17)
Fe1−O3	2.066(4)	N4−Fe1−N9	80.44(19)
Fe1−N4	2.129(5)	N9−Fe1−N7	70.88(19)
Fe1−N9	2.139(5)	N4−Fe1−N5	71.73(18)
Fe1−N7	2.147(5)	N7−Fe1−N6	68.71(18)
Fe1−N5	2.180(5)	N5−Fe1−N6	68.41(17)
Fe1−N6	2.250(5)		

4, and important bond distances are listed in Table 4. The octahedral Ni(II) ions are bound to two ligands, with a combination of N_2 bidentate and N_2O tridentate pockets at each metal center (Chart 2c). The sixth coordination site is occupied by an acetonitrile molecule in each case. Two protons are found on each ligand (H(1) and H(2) bound to N(5) and N(7), respectively) indicating ligand neutrality in keeping with the presence of four perchlorate anions. The C−O(2) bond is short (1.241(4) Å) and so is a formal C=O bond, in keeping with the long Ni(1)−O(2) distance (2.1586-(19) Å). The two central pyridine rings of each ligand are uncoordinated, and the overall dinuclear structural arrangement brings these rings into a roughly parallel, but displaced arrangement (closest contact 4.94 Å between the pyridine nitrogen atoms). A similar structure was observed for the complex [Ni2(2poap)2(H2O)2](NO3)4.[20]

[Ni2(Cl2poap)3F](BF4)3·5H2O (4). The structure of the dinuclear cation in **4** is shown in Figure 5, and important bond distances are listed in Table 5. The dinuclear structure differs dramatically from that in **3**, in that three spirally

around the metal ion, leaving open the possibility of further external coordination.

[Cu(SEt2poap)(ClO4)](ClO4)(CH3CN) (2). The molecular structure of the mononuclear cationic fragment in **2** is shown in Figure 3, and important distances and angles are listed in Table 3. Complex **2** was formed in reasonable yield from a reaction mixture which included Mn(ClO4)2, in an attempt to synthesize a mixed-metal grid (Chart 2b). The copper center effectively binds to one-half of the ligand, but in a slightly different coordination mode compared with that of **1**. The ligand is tetradentate (N3O) and neutral, as indicated by the presence of two perchlorates. One perchlorate is bonded to an axial copper site via O(6) with a long contact (2.444(3) Å), thus creating a square-pyramidal copper geometry. In-plane Cu−N and Cu−O distances are much shorter (1.970(3), 1.944(4), and 1.948(3) Å for N(1), N(3), and N(5), respectively; Cu(1)−O(1) 1.958(3) Å). Ligand protons are located at N(7) and O(2) sites, confirming the neutrality of the ligand. Examination of the bond lengths within the O−C−N−N−C−N framework reveals that there is significant electron delocalization, and so the observed distances are not always in agreement with normal double and single bonds. The ligand itself adopts an almost flat conformation throughout, brought about by copper coordination on one side and the electron delocalization effect on the other side.
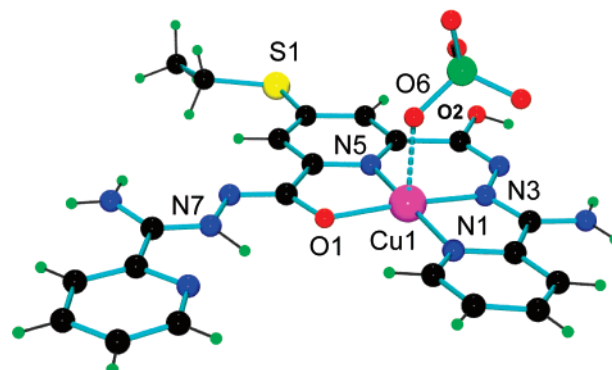
[Ni2(2pmoap)2(CH3CN)2](ClO4)4·4H2O (3). The molecular structure of the dinuclear cation in **3** is shown in Figure

Figure 3. POVRAY structural representation of the cation in **2**.

Table 3. Bond Lengths (Å) and Angles (deg) for **2**

Cu1−N3	1.944(4)	N3−Cu1−N5	91.51(14)
Cu1−N5	1.948(3)	N3−Cu1−O1	171.76(13)
Cu1−O1	1.958(3)	N5−Cu1−O1	84.38(13)
Cu1−N1	1.970(3)	N3−Cu1−N1	83.43(15)
		N5−Cu1−N1	172.95(14)
		O1−Cu1−N1	100.01(14)
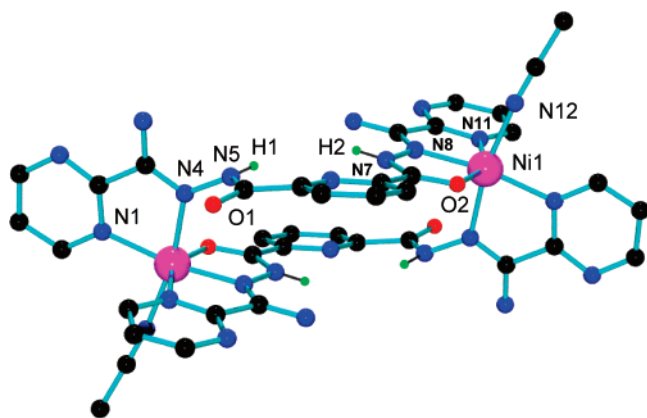
Figure 4. POVRAY structural representation of the cation in **3**.

Table 4. Bond Distances (Å) for **3**

Ni1−N8	2.007(2)
Ni1−N12	2.059(3)
Ni1−N4	2.061(2)
Ni1−N1	2.086(2)
Ni1−N11	2.118(2)
Ni1−O2	2.1586(19)

arranged neutral bis-bidentate ligands wrap around a triad of two metals and a fluoride ion. This arrangement is rare, but has been observed before in the complex $[Ni_2(2pzoap)_3F]$-$(BF_4)_3\cdot8.5H_2O^{19a}$ and involves terminal six-coordinate Ni-(II)N_6 ions bound at the congruence of the N_2 end pockets of three ligands (Chart 2d), with a fluoride ion occupying the central metal-free cavity, bound by six well-defined hydrogen bonds to hydrogen atoms attached to hydrazone nitrogen atoms N(4), N(6), N(13), N(15), N(22), and N(24) in a pseudo-octahedral shape. F−H−N angles fall in the range of 137.5−140.7°, with F−N distances in the range of 2.73−2.88 Å. The ligands adopt a syn conformation at the central pyridine rings, with the hydrazone oxygens external to the central cavity. C−O bond distances fall in the range of 1.22−1.24 Å, indicating C=O double-bond character. The appearance of adventitious fluoride presumably results from the hydrolysis of BF_4^-, leading to HF and $BF_3(OH)^-$.[19b]

$[Fe_2(2popp)_3F](PF_6)_3\cdot2H_2O$ (5). The structure of the cation in **5** is shown in Figure 6, and relevant bond distances are listed in Table 6. The cation has a spiral-like structure similar to that of **4**, with each Fe(II) center occupying an N_6 coordination pocket, again resulting from the congruence of three terminal N_2 ligand fragments (Chart 2d). Fe−N distances are very short and fall in the range of 1.93−1.98 Å, suggesting a low-spin Fe(II) system (vide infra), which would be compatible with the N_6 environment created by the ends of the three ligands. However, a redox reaction must have occurred in order to produce Fe(II), since the initial reaction involved $Fe(III)(ClO_4)_3\cdot6H_2O$ as starting material. This is reasonably associated with a small amount of ligand hydrolysis in the methanolic solvent mixture, producing reducing hydrazide fragments, which would reasonably occur at the terminal imine groups. This has been observed before, but with ligands containing amidrazone type ends (e.g., Cl2poapz).[37]

The Fe centers are well-separated in **5** (7.892(3) Å), with the ligands oriented with the diazine N_2 groups pointing
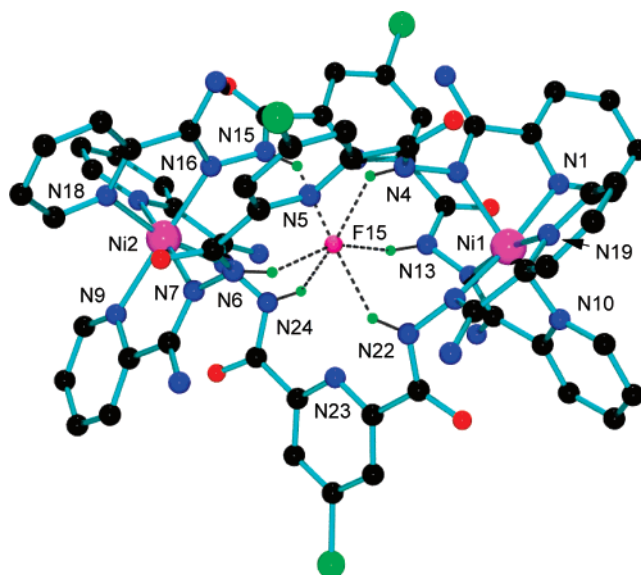

Figure 5. POVRAY structural representation of the cation in **4**.

Table 5. Bond Distances (Å) for **4**

Ni1−N12	2.0500(19)	Ni2−N25	2.0297(19)
Ni1−N3	2.053(2)	Ni2−N7	2.0596(19)
Ni1−N21	2.059(2)	Ni2−N16	2.0655(19)
Ni1−N19	2.079(2)	Ni2−N18	2.0899(19)
Ni1−N1	2.099(2)	Ni2−N27	2.0902(19)
Ni1−N10	2.102(2)	Ni2−N9	2.1095(19)

inward and in tautomeric forms in which the C−O bonds have significant ketonic character (C−O 1.20−1.23 Å). This arrangement leaves a large cavity in the central portion of the structure. The neutral ligand protons are located on nitrogen atoms N(3), N(5), N(9), N(10), N(17), and N(19), which point inward, within the cavity, and remarkably again a fluoride ion is encapsulated within the cavity by six hydrogen-bonding contacts to these nitrogen atoms (F−N 2.80−2.91 Å). The driving force for this structural arrangement would include the opportunistic fluoride ion and its nice fit within the cavity, but also the desire of the low-spin Fe(II) centers to have a suitable N_6 coordination environment. However, in this case the fluoride clearly must result from the hydrolysis of PF_6^-. The steric bulk of the phenyl rings at the ends of the ligand causes a pronounced distortion of the Mn(II)$_9$ [3 × 3] grid formed with this ligand,[15] and this steric effect may serve also to hinder the expected grid formation in the present case.

$[Fe_2(2popp)_3Cl](ClO_4)_3\cdot6H_2O$ (6). The dinuclear cation in **6** is shown in Figure 7, and relevant bond distances are listed in Table 7. Two perchlorate anions show up clearly in the structure, but the third perchlorate is somewhat disordered. Three bis-bidentate ligands are bound around the two iron atoms in the same way as in **4** and **5** (Chart 2d). Six ligand protons show up in difference maps on diazine nitrogen atoms N(3), N(5), N(10), N(12), N(17), and N(19), indicating the neutral nature of the three ligands and that the di-iron cation bears a +3 charge. The structure of **6** is

(37) Kelly, T. L.; Milway, V. A.; Grove, H.; Niel, V.; Abedin, T. S. M.; Thompson, L. K.; Zhao, L.; Harvey, R. G.; Miller, D. O.; Leech, M.; Goeta, A. E.; Howard, J. A. K. *Polyhedron* **2005**, *24*, 807.
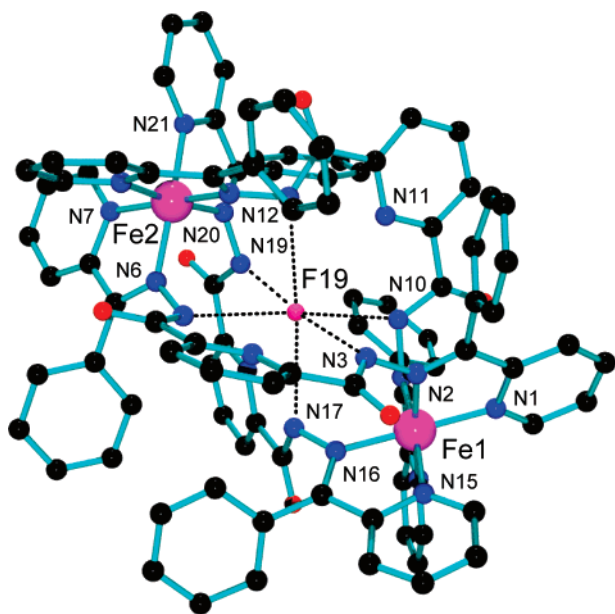
Figure 6. POVRAY structural representation of the cation in **5**.

Table 6. Bond Distances (Å) for **5**

Fe1—N9	1.933(4)	Fe2—N21	1.952(4)
Fe1—N2	1.934(4)	Fe2—N14	1.967(4)
Fe1—N16	1.936(4)	Fe2—N7	1.967(4)
Fe1—N15	1.968(4)	N2—N3	1.412(5)
Fe1—N1	1.969(4)	N5—N6	1.408(5)
Fe1—N8	1.974(4)	N9—N10	1.407(5)
Fe2—N13	1.938(4)	N12—N13	1.409(5)
Fe2—N20	1.946(4)	N16—N17	1.411(5)
Fe2—N6	1.949(4)	N19—N20	1.407(5)

similar to that of **4** and **5**, which both contain a fluoride ion in the central cavity. Fe—N distances (1.93–1.98 Å) are very short, and once again consistent with iron(II) ions in the low-spin state (vide infra) (cf. **5**). In the case of **6**, there is a central atom occupying the same site as that of the F⁻ ion in **4** and **5**, and it is assigned reasonably as a Cl⁻ ion. The source of adventitious chloride in this compound is puzzling, but the commercially available Fe(III) perchlorate used (Aldrich) contains a small percentage of chloride. This seems to be a more reasonable source rather than chloroform (solvent) or perchlorate itself. These nitrogen atoms point inward within the central cavity in the structure and take part in hydrogen bonding to the chloride ion Cl(3) (Cl—N 3.0–3.5 Å) in a fashion similar to that of the F⁻ ion in **4** and **5**. The presence of Fe(II) again suggests that some ligand hydrolysis must have occurred to reduce the Fe(III) starting material, but the complex contains the starting ligand, as in **5**. The presence of Cl⁻ in the middle of the cavity of the cation may be considered as one of the driving forces for the formation of this type of complex, where it could act as a possible anionic templating species in the assembly process. However, the choice of the N_6 ligand environment for the Fe(II) sites and the presence of bulky ligand end pieces must again also contribute to the formation of a dinuclear system rather than a grid and provide a suitable donor grouping to stabilize the low-spin state.

[Ni₆(SEt2poap-H)₅](CF₃SO₃)₇·14H₂O (7). The structure of the hexanuclear cation in **7** is shown in Figure 8, and
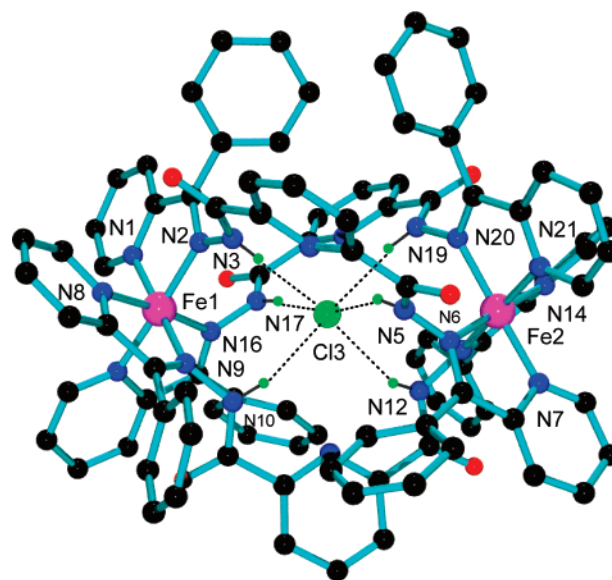

Figure 7. POVRAY structural representation of the cation in **6**.

Table 7. Bond Lengths (Å) for **6**

Fe1—N16	1.935(5)	Fe2—N6	1.946(6)
Fe1—N2	1.949(5)	Fe2—N21	1.949(7)
Fe1—N1	1.964(5)	Fe2—N13	1.952(6)
Fe1—N15	1.965(6)	Fe2—N7	1.965(6)
Fe1—N8	1.966(5)	Fe2—N20	1.969(6)
Fe1—N9	1.971(6)	Fe2—N14	1.980(6)

important bond distances and angles are listed in Table 8. Six pseudo-octahedral Ni(II) centers are bound to five ligands in a $2 \times [1 \times 3]$ rectangular array, with two groups of three metal ions coordinated in a linear trinuclear fashion to a single ligand, all bridged by hydrazone oxygen atoms (Chart 1). Ni—O—Ni angles fall in the range of 137–141 °. These two ligands utilize three coordination pockets providing a mer-ligand environment at each Ni(II) center. Three other ligands straddle the tri-nickel subunits in a roughly parallel arrangement and bridge them providing mer-N_2O donor groupings to complete the six-coordinate metal-ion coordination spheres. However, an unusual twist in each ligand occurs, such that one bridging ligand end adopts the normal N_2O grouping, but the other has a 180° twist to effectively provide the same N_2O pocket, but in an anti conformation (Chart 2e). This can be seen more clearly in Figure 9, which also highlights the core structural arrangement. This overall structure leaves the central pyridine rings of the straddling ligands uncoordinated, but there is evidence from the full structure for some solvent (water) occupancy of the central cavities, which may help to stabilize this unusual incomplete rectangular grid structure.

This unusual structural arrangement creates two essentially isolated trinuclear Ni_3-(μ-O)$_2$ halves separated by large distances. Ni—Ni separations fall in the range of 3.94–4.07 Å within each trinuclear subunit and 9.08–9.61 Å across the rectangle. The presence of seven clearly defined triflate anions in the lattice leads to an overall charge balance requiring a total of five negative charges on the five ligands. Pinpointing sites of deprotonation is difficult at the current refinement level. CO bonds in the three lateral ligands fall
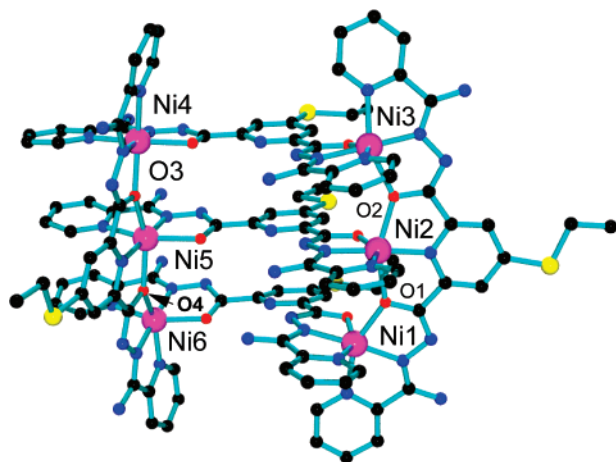
Figure 8. POVRAY structural representation of the cation in **7**.

Table 8. Bond Lengths (Å) and Angles (deg) for **7**

Ni1−N3	1.966(5)	Ni4−N10	2.106(5)
Ni1−N25	1.993(5)	Ni4−O9	2.107(4)
Ni1−N27	2.061(5)	Ni4−O3	2.110(4)
Ni1−O1	2.114(4)	Ni5−N30	1.954(5)
Ni1−N1	2.119(5)	Ni5−N14	1.981(5)
Ni1−O6	2.203(5)	Ni5−N28	2.132(5)
Ni2−N5	1.978(5)	Ni5−O3	2.166(4)
Ni2−N34	2.001(4)	Ni5−O7	2.169(4)
Ni2−O2	2.119(4)	Ni5−O4	2.170(4)
Ni2−O1	2.130(4)	Ni6−N16	1.949(5)
Ni2−N36	2.135(5)	Ni6−N21	2.000(5)
Ni2−O8	2.144(5)	Ni6−N19	2.081(6)
Ni3−N7	1.942(5)	Ni6−O5	2.110(4)
Ni3−N43	1.985(5)	Ni6−N18	2.122(5)
Ni3−N45	2.061(5)	Ni6−O4	2.149(4)
Ni3−N9	2.090(5)		
Ni3−O2	2.108(4)	Ni1−O1−Ni2	138.6(2)
Ni3−O10	2.216(4)	Ni3−O2−Ni2	137.79(19)
Ni4−N12	1.946(5)	Ni4−O3−Ni5	138.7(2)
Ni4−N39	1.985(5)	Ni6−O4−Ni5	140.6(2)
Ni4−N37	2.066(5)		

in the range of 1.23−1.29 Å, implying significant C=O double-bond character, while the other CO bonds are somewhat longer (1.30−1.32 Å), suggesting more single-bond character.

[Ni$_6$(Cl2poap-2H)$_5$](BF$_4$)$_4$[Ni(H$_2$O)$_6$]·20H$_2$O (8). The structure of the cation in **8** is shown in Figure 10, and important bond distances and angles are listed in Table 9. The structure reveals a hexanuclear cation with six octahedral Ni(II) ions bound in a 3 + 3 arrangement similar to that found in **7**. Superficially, the structures appear to be the same, with equivalent complex cation stoichiometry, but on close examination the arrangement of the three straddling ligands is different, with a syn rather than anti conformation (Chart 2f). No solvent molecules were detected in the empty central ligand compartments. Also, a [Ni(H$_2$O)$_6$]$^{2+}$ cation was located on a special position in the lattice, with no tangible connection to the hexanuclear cation, and appears to have resulted adventitiously, perhaps in response to a charge balance.

Ni−Ni separations within each trinuclear half fall in the range of 3.97−4.03 Å, typical of systems in this class, where the metals ions are bridged by hydrazone oxygen atoms. Ni−Ni distances across the straddling ligands are much larger (9.9−10.5 Å). Ni−O−Ni bridge angles fall in the range of 138−140°, typical of [3 × 3] grids with this ligand. The
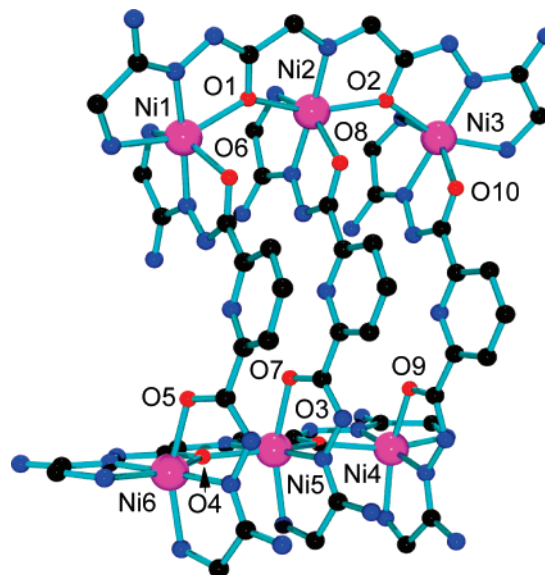
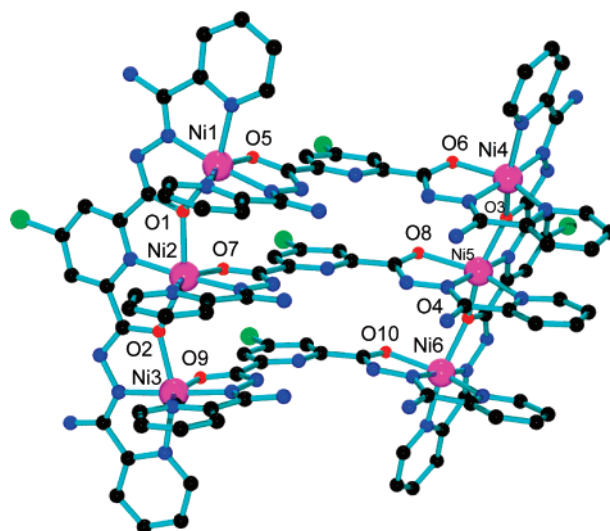**Figure 9.** Abbreviated POVRAY structural representation of the cation in **7**.

Figure 10. POVRAY structural representation of the cation in **8**.

overall charge balance requires that each ligand formally loses two protons. For the two tritopic ligands, this would be associated largely with proton loss at the hydrazone oxygen atoms (C−O distances >1.3 Å). For the ditopic ligands, short CO distances (1.23−1.26 Å) indicate significant C=O double-bond character and that proton loss is associated with the diazine nitrogen atoms.

[Co$_7$(2poap-2H)$_5$](ClO$_4$)$_8$·5CH$_3$CN·11H$_2$O (9). The structure of the heptanuclear cation in **9** is shown in Figure 11, and relevant bond distances and angles are listed in Table 10. It is similar to **7** and **8** in that it has two trinuclear fragments involving one ligand bound to three metal ions (Co(1)−Co(4)−Co(6) and Co(3)−Co(5)−Co(7)), with the two trinuclear fragments cross-linked by three lateral ligands, which complete the cobalt coordination spheres in a meridional fashion via their end pockets. This arrangement creates additional pockets in the central portion of the "pseudo-grid"-like arrangement, and in this case one of these is occupied by a seventh metal ion Co(2) (Chart 2g), which is bonded

Table 9. Bond Lengths (Å) and Angles (deg) for **8**

Ni1−N3	1.941(4)	Ni4−O6	2.118(4)
Ni1−N21	1.975(4)	Ni5−N14	1.987(5)
Ni1−N19	2.067(5)	Ni5−N34	1.997(5)
Ni1−N1	2.103(5)	Ni5−N36	2.071(5)
Ni1−O1	2.117(4)	Ni5−O4	2.123(4)
Ni1−O5	2.146(4)	Ni5−O3	2.147(4)
Ni2−N5	2.007(4)	Ni5−O8	2.210(4)
Ni2−N30	2.017(5)	Ni6−N16	1.948(5)
Ni2−N28	2.076(5)	Ni6−N43	1.983(5)
Ni2−O2	2.130(4)	Ni6−N45	2.072(5)
Ni2−O7	2.153(4)	Ni6−N18	2.125(6)
Ni2−O1	2.173(4)	Ni6−O4	2.134(4)
Ni3−N7	1.950(5)	Ni6−O10	2.146(4)
Ni3−N39	1.968(5)	Ni1−O1−Ni2	139.37(18)
Ni3−N37	2.081(6)	Ni3−O2−Ni2	139.18(19)
Ni3−N9	2.105(6)	Ni4−O3−Ni5	138.3(2)
Ni3−O2	2.113(4)	Ni5−O4−Ni6	138.9(2)
Ni3−O9	2.128(4)		
Ni4−N12	1.958(5)		
Ni4−N25	1.968(5)		
Ni4−N27	2.082(6)		
Ni4−O3	2.103(4)		
Ni4−N10	2.114(5)		

Table 10. Bond Lengths (Å) and Angles (deg) for **9**

Co1−N30	1.833(5)	Co5−N16	1.997(5)
Co1−N3	1.846(5)	Co5−N41	2.062(5)
Co1−O1	1.919(4)	Co5−O4	2.087(4)
Co1−N1	1.930(6)	Co5−N18	2.173(6)
Co1−N28	1.934(5)	Co5−O9	2.272(4)
Co1−O7	1.958(4)	Co5−O10	2.275(4)
Co2−O12	2.031(5)	Co6−N34	1.839(5)
Co2−O11	2.057(4)	Co6−N21	1.864(5)
Co2−N5	2.065(5)	Co6−O5	1.909(5)
Co2−N46	2.089(6)	Co6−N19	1.932(6)
Co2−O2	2.223(4)	Co6−N36	1.941(5)
Co2−N4	2.240(5)	Co6−O8	1.976(4)
Co3−N7	1.848(5)	Co7−N25	1.853(5)
Co3−N39	1.849(5)	Co7−N43	1.854(5)
Co3−N9	1.920(5)	Co7−O6	1.930(4)
Co3−N37	1.926(5)	Co7−N45	1.934(5)
Co3−O2	1.928(4)	Co7−N27	1.938(5)
Co3−O9	1.936(4)	Co7−O10	1.952(4)
Co4−N12	2.014(5)	Co1−O7−Co4	142.0(2)
Co4−N32	2.034(5)	Co3−O2−Co2	138.4(2)
Co4−N10	2.106(6)	Co3−O9−Co5	139.8(2)
Co4−O3	2.149(5)	Co6−O8−Co4	143.1(2)
Co4−O7	2.248(4)	Co7−O10−Co5	140.0(2)
Co4−O8	2.341(4)		

to the central pyridine nitrogen of one cross-linking ligand and adjacent hydrazone oxygen and nitrogen atoms in a meridional fashion, with two water molecules and an acetonitrile occupying the other octahedral sites. The lateral ligands again adopt the anti conformation, binding to two cobalt ions via N_2O end pockets (Chart 2e), thus projecting the cobalt triads on opposite sides of the group of lateral ligands. This is of course in complete contrast to the way in which one would envisage the normal [3 × 3] grid assembly occurring, but clearly emphasizes the fact that there are other stable ligand conformational arrangements, which form multinuclear aggregates.
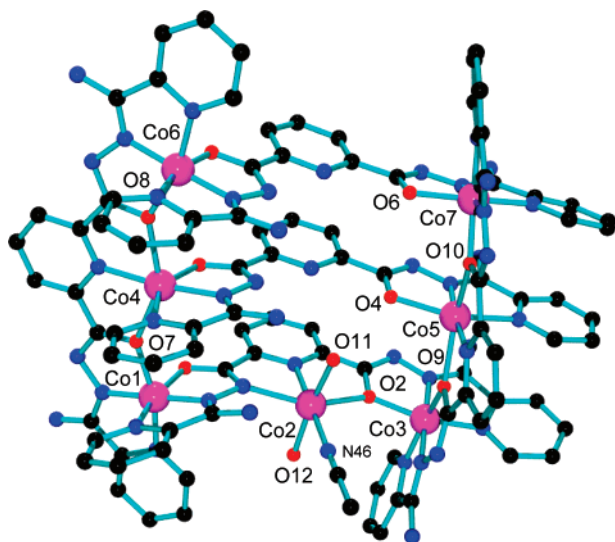
An examination of the Co−ligand distances reveals four cobalt centers with very short bonds. Co(1), Co(3), Co(6), and Co(7) have averaged Co−L distances of 1.902(5), 1.919-(5), 1.913(5), and 1.910(5) Å, respectively, clearly indicating that these are Co(III) centers. Co−L distances for Co(2), Co-(4), and Co(5) (2.111, 2.153, and 2.140 Å averages, respectively) are more typical of those of Co(II). These distances compare closely with those observed in the related

Figure 11. POVRAY structural representation of the cation in **9**.

tetranuclear complex [Co(II)$_2$Co(III)$_2$(poap)$_4$(H$_2$O)$_2$(MeOH)$_2$]-(NO$_3$)$_4$ (Co(III)−L 1.906 Å(ave.), Co(II)−L 2.112 Å(ave.)).[6] These assignments are also supported by bond valence sum (BVS) calculations.[38] BVS values for Co(2), Co(4), and Co-(5) (2.19, 2.15, and 2.14, respectively) clearly indicate Co-(II). However the high values for the remaining sites (4.00−4.11) are typical of Co(III) in this sort of ligand environment.[6] The reaction of the ligand 2poap with Co(ClO$_4$)$_2$·6H$_2$O was not carried out in an oxygen-free atmosphere, and the recrystallized sample was not protected from air, indicating the oxygen sensitivity of such systems. Such an arrangement with the oxidized metal ions at extreme sites (corner sites) is of interest, since Mn(II)$_9$ grids with related ligands (e.g., [Mn$_9$(2poap-2H)$_6$](ClO$_4$)$_6$·18H$_2$O) can be electrochemically and chemically oxidized to form mixed-oxidation-state grid species Mn(II)$_x$Mn(III)$_{9-x}$ (x = 5, 6), in which the first metal centers to oxidize are those located in equivalent corner grid positions.[15,39]

[Ni$_9$(Cl2popp)$_5$(OH)$_2$(CH$_3$CN)$_2$(H$_2$O)$_3$](ClO$_4$)$_6$·19H$_2$O (10). A partial structure was obtained for complex **10**, but poor refinement due to a limited diffraction data set prevents a report of any accurate details at this time (refinement >25%). However, the grid framework is clearly revealed, and nine metal sites are occupied, arranged in the normal square [3 × 3] [Ni$_9$-(μ-O)$_{12}$] arrangement, with the ligands in their syn conformation. However, only five ligands are present, in keeping with the structures of **7**−**9**. One ligand is missing from the central portion of the grid, but three nickel ions occupy the coordination sites with additional terminal co-ligands (CH$_3$CN and water) and what appear to be hydroxide ions bridging the central Ni to its neighbors. Overall grid dimensions are comparable with other nonanuclear square [3 × 3] grids in this class. The elemental

(38) (a) Palenik, G. J. *Inorg Chem.* **1997**, *36*, 122. (b) O'Keefe, M.; Brese, N. E. *J. Am. Chem. Soc.* **1991**, *113*, 3226.
(39) Thompson, L. K.; Kelly, T. L.; Dawe, L. N.; Grove, H.; Lemaire, M. T.; Howard, J. A. K.; Spencer, E. C.; Matthews, C. J.; Onions, S. T.; Coles, S. J.; Horton, P. N.; Hursthouse, M. B.; Light, M. E. *Inorg. Chem.* **2004**, *43*, 7605.

analysis (see Experimental Section) and the magnetic properties (vide infra) are entirely consistent with this preliminary structure.

Mechanism of Grid Formation. The tritopic hydrazone ligands (Chart 1) nominally have two readily ionizable protons, and these may be associated with oxygen or nitrogen atoms in the hydrazone backbone depending on the ligand conformation. The pH associated with the solvent medium may then be an important factor in determining not only the charge on the ligand but also its geometric conformation. Chart 2 highlights the different coordination modes for ligands in this class observed in this study, indicating the complexity of the bonding situation and the difficulties involved in controlling it. The most commonly observed conformational mode involves the syn-enolic arrangement of the ligand ends, which aligns three tridentate coordination pockets, thus creating five-membered chelate rings and μ-O bridging between the three metal ions (Chart 1). This is clearly the important conformational ligand mode required for normal [3 × 3] grid self-assembly.

[3 × 3] nonanuclear grids, with μ-O bridging between metal ions, have so far occurred as the dominant outcome with a variety of ligands in this class with, e.g., Mn-(II), Cu-(II), and Zn(II) salts, suggesting that this grid arrangement is the thermodynamically favored product with these metal ions (Scheme 1). Clearly, a match of the size of the cation, its coordination requirements, and the nature of the coordination pocket into which it fits are factors which control whether the combination is a good one and perhaps whether a grid will be the most likely outcome. A few simple 1:3 trinuclear copper(II) complexes have been produced, but with the alternate μ-NN bridging mode, and they seem to occur only when there is ligand competition, e.g., from potentially coordinating anionic groups and possibly the solvent.[21] Another stable oligomeric structural arrangement is the pinwheel cluster (Scheme 1), which forms, so far, just with copper(II) and, e.g., 2poap, Cl2poap, and Cl2pomp, but requires the use of solvent mixtures which largely exclude water and reactions without heating.[17,18] However, it involves the μ-O-bridged triad arrangement of three Cu(II) centers per ligand typical of the grids. The fact that the coordination requirements of copper(II) do not always involve six ligands (e.g., four- and five-coordinate geometries are quite stable) may be a significant factor in the outcome with copper, although [3 × 3] grids involving six-coordinate copper centers do form readily, even though some coordination spheres have quite distorted geometries.

The present study shows that partial grids frequently form with cobalt (Co$_7$) and nickel (Ni$_6$) salts (compounds **7–9**), and in all cases some of the ligands adopt conformations (syn or anti), which would effectively prevent normal [3 × 3] [M$_9$-(μ-O)$_{12}$] grid formation, because of the ligand twist and the external positioning of the hydrazone oxygen groups. However, in the syn conformation (Chart 2f) a metal could occupy the central cavity to create a linear μ-NN-bridged metal triad, with the subsequent formation of a rectangular grid with μ-O bridges on the ends and μ-NN bridges along the sides. This has been achieved recently with the 3 × [1

× 3] symmetric rectangular grid [Mn$_9$(L1)$_6$](ClO$_4$)$_6$·8H$_2$O (Chart 1), which involves the bulky quinoline ligand L1, with three [Mn$_3$(μ-O)$_2$] subunits linked by three (μ-NN) (Chart 2e) subunits (Figure S1, Supporting Information).[40]

The formation of the hexametallic and heptametallic partial grids clearly suggests that they represent coordination options among a large number of possible oligomeric intermediates or grid fragments. Square Ni$_9$ and Co$_9$ [3 × 3] M$_9$L$_6$ hydrazone oxygen-bridged grids have not yet been characterized structurally, and with the exception of **10**, which is a [3 × 3] grid, but with only five ligands, only grid fragments have been produced. This may indicate that the nature of the metal ion, its crystal field requirements and Lewis acid characteristics, is more important for these metals than for Mn(II), where grids form with ease as the exclusive products and crystal field effects are not relevant. Complex **9** indicates that despite the anti-ligand twist (Chart 2g), an extra metal can occupy a central grid site, and in principle an asymmetric rectangular M$_9$ grid is possible with this ligand combination. However, in this case the mixture of Co(II) and Co(III) sites complicates the situation and begs the question as to whether oxidation occurred during partial grid assembly or after the partial grid was formed.

The common structural features of compounds **7–9**, involving the μ-O-bridged linear trinuclear end fragments, suggests that the first step in grid formation may be the complexation of one ligand with three metal ions. Solvent or anions may occupy the additional metal ions' sites in such an intermediate species. Other ligand ends would then assemble to complete the mer octahedral metal coordination spheres and thus organize three additional ligands at right angles to the triad, with some empty external coordination compartments. Depending on kinetic factors and the reaction pH conditions, these ligand ends may then have the conformational freedom to adopt different orientations. Another trinuclear fragment could then bind in a similar fashion at the assembly of similar empty end pockets to form a rectangular arrangement, followed by the incorporation of three metals in the central pocket arrangement, accompanied by an extra ligand. What is interesting in this context is the fact that in **7–9** the central and peripheral aromatic rings of the lateral ligands adopt pseudo-eclipsed parallel arrangements, indicating that conformational freedom is apparently somewhat limited due to the likely presence of $\pi-\pi$ interactions. The choice of the conformation of the secondary ligands will dictate whether or not [M$_9$-(μ-O)$_{12}$] will be the favored outcome, but complexes **7–9** clearly indicate other viable self-assembly options. The formation of the rectangular grid [Mn$_9$(L1)$_6$](ClO$_4$)$_6$·8H$_2$O (Figure S1, Supporting Information) suggests that steric bulk associated with the ligand ends may be a significant factor in determining which ultimate ligand conformation is chosen and that μ-NN bridging arrangements within the grid are reasonable options.

The mononuclear complex **1** shows that the ligand Cl2poapz can wrap around a single metal cation to present

(40) Dey, S. K.; Abedin, T. S. M.; Dawe, L. N.; Tandon, S. S.; Collins, J. L.; Thompson, L. K.; Postnikov, A. V.; Alam, M. S.; Müller, P. *Inorg. Chem.* **2007**, *46*, 7767.

five nitrogen donor sites in a planar pentadentate arrangement. Fe(III) is capable of adopting a pentagonal-bipyramidal structure in order to accommodate such an arrangement. The low yield of this product suggests that other species, as yet unidentified, may be present in the reaction solution. In the case of **2**, the mononuclear structure again represents a comfortable ligand fit for Cu(II), indicating other simple coordination options. Complexes **3**−**6** form two different dinuclear structural types. Complex **3** has two remote Ni(II) centers bridged by two ligands via N_2 and N_2O coordination pockets. Complexes **4**−**6** have common and unusual spiral dinuclear structures with N_2 ligand ends converging to form MN_6 metal centers. The inner pocket created by such an arrangement attracts F^- and Cl^- ions. Rationalizing the formation of such species is difficult, particularly since redox reactions are involved with **5** and **6**, but previous work on ligands in this class indicates that metal-ion-promoted hydrolysis/solvolysis can occur, producing hydrazone fragments, which have the potential to act as reducing agents.[37] Clearly, these unusual structural examples are an indication of the overall complexity of the coordination chemistry involved with this class of tritopic ligand, and while there have been many straightforward examples, particularly with Mn(II) and Cu(II), reactions with other metals indicate that there are many other coordination options, including [3 × 3] grid formation. A rare example of a [3 × 3] grid with nickel(II) (**10**) shows that the grid framework can be stable in the absence of one ligand, which might have been regarded as a vital structural element. This highlights the thermodynamic stability of the grid core as a whole and begs the question as to whether it could be constructed from simpler building blocks.

Crystal field effects, metal-ion charge and size, preferred anisotropic character, and redox behavior are among the important metal properties one should consider when assessing the consequences of incorporating a particular ion into a grid site. Site preferences will differ based on donor composition and the site cavity size, resulting from the metal-ion bonding requirements and the various electrostatic forces which control how the ligands assemble. Homovalent grids $(M(II)_9)$ are common, but while the incorporation of M(III) ions has been documented with Mn mixed-oxidation-state [3 × 3] grids, $M(III)_9$ grids have so far not been structurally characterized. The smaller ionic radii involved may create ligand congestion and thus effectively hinder full grid assembly. This could lead to simpler options or, as in the case of **5** and **6**, reduction followed by the assembly of ligand donor sites more suited to low-spin Fe(II) centers. The unusual incomplete grid complex $[Fe(III)_5(Cl2poap)_6](ClO_4)_9$ is perhaps an illustration of the ionic radius limitation (Figure 12). Fe(III) ions are incorporated symmetrically in the corner and central positions, within a ligand framework which is essentially the same as that in the normal [3 × 3] grids.[14] The complementary fit of the six ligands indicates the comfortable arrangement of the parallel ligand triads, and the presence of π-interactions between the aromatic rings.

Magnetic Properties. The variable-temperature magnetic properties of **1** show an essentially constant moment from

room temperature (5.83 μ_B) to about 10 K, with a slight drop below 10 K. This confirms the presence of a single high-spin Fe(III) center, and the slight drop below 10 K is associated with zero field splitting effects. Complex **2** has a normal magnetic moment for a mononuclear Cu(II) complex. Complex **3** has an essentially constant moment of 4.5 μ_B per mol down to ∼12 K, followed by a slight drop at lower temperature, associated with zero field splitting effects. The remote location of the Ni(II) ions does not lead to any magnetic exchange. Complex **4** exhibits essentially identical magnetic properties in agreement with the well-separated Ni-(II) centers. Complexes **5** and **6** have moments of essentially zero in the range of 2−300 K, indicating low-spin Fe(II) compounds. This can be attributed to the strong N_6 ligand field generated by the N_2 ends of the three ligands bound to each Fe(II) center. These compounds are similar to simpler dinuclear (2:3 metal/ligand) Fe(II) systems with the ligands PAHAP and PZHPZ (bis-picolinamide azine and bis-pyrazinamide azine, respectively), which have low-spin Fe-(II) centers and similar N_6 coordination environments at the metal sites.[41]

Complex **7** has six Ni(II) centers arranged in two spatially isolated trinuclear arrays (Figures 8 and 9), and it is reasonable to assume that any magnetic communication between these subunits will be weak. Within each trinuclear grouping the Ni(II) centers are bridged by single hydrazone oxygen atoms, with large Ni−O−Ni angles. Therefore, antiferromagnetic coupling would be expected between the three Ni(II) centers. The exchange Hamiltonian for this system (eq 1 and Figure 13) is based on two isolated linear

$$H_{ex} = -J(S_1S_2 + S_2S_3 + S_4S_5 + S_5S_6) \qquad (1)$$

$$\chi_M = \frac{N\beta^2g^2}{3k(T-\theta)} \frac{\sum S'(S'+1)(2S'+1)e^{-E(S')/kT}}{\sum(2S'+1)e^{-E(S')/kT}}(1-\rho) + \frac{N\beta^2g^2S(S+1)\rho}{3kT} + TIP \quad (2)$$

trinuclear $Ni(II)_3$ subunits with a single *J* value. The magnetic profile for **7** is shown in Figure 14. The molar magnetic moment of 7.9 μ_B at 300 K is reasonable for six Ni(II) centers and drops to 3.3 μ_B at 2 K, characteristic of intramolecular antiferromagnetic coupling. The magnetic data were fitted to eq 1 using an appropriate vector coupling approach, within *MAGMUN,* version 4.1, which substitutes the total spin state/energy situation into the modified van Vleck equation (eq 2) (TIP = temperature-independent paramagnetism, ρ = fraction of paramagnetic impurity, θ = Weiss-like temperature correction).[42] The best fit of the data gave g_{av} = 2.252-(9), *J* = −8.8(4) cm^{-1}, TIP = 1360 × 10^{-6} cm^{-3}•mol^{-1}, ρ = 0.004, θ = −1.4 K, 10^2R = 0.92 (R = [$\sum(\chi_{obs}-\chi_{calc})^2/\sum\chi_{obs}^2]^{1/2}$) (solid line in Figure 14). The value of μ_{mol} at 2 K is somewhat below the expected ground-state value for these fitted parameters (4.5 μ_B). The necessity for inclusion of a small negative θ value suggests that there may be an

(41) Xu, Z.; Thompson, L. K.; Miller, D. O.; Clase, H. J.; Howard, J. A. K.; Goeta, A. E. *Inorg. Chem.* **1998**, *37*, 3620.
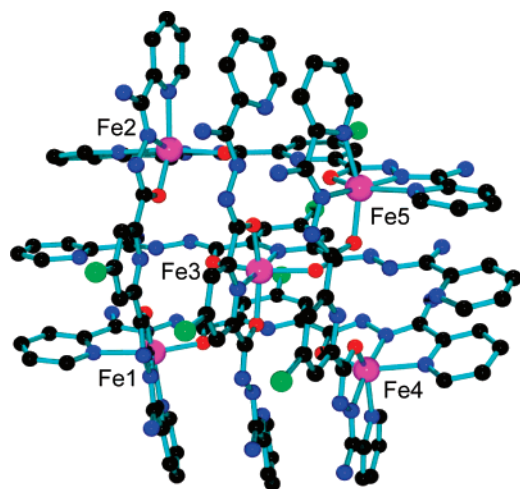
Figure 12. POVRAY structural representation of the cation in [Fe₅-(Cl2poap)₆](ClO₄)₉.
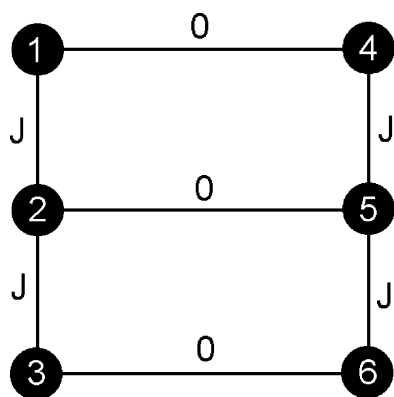

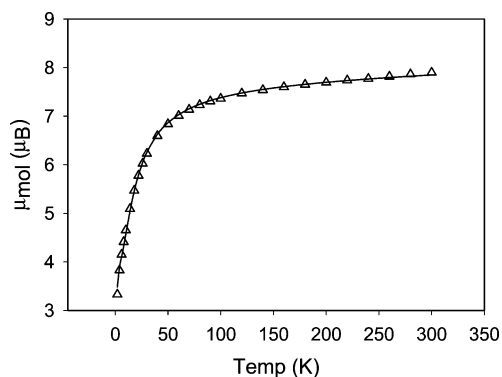**Figure 13.** Magnetic exchange model for the hexanuclear nickel framework in **7**.

Figure 14. Variable-temperature magnetism for **7** (see text for fitted parameters).

additional antiferromagnetic interaction at play, perhaps a long-range interaction between the Ni(II)₃ subunits via the straddling ligands. There is no structural evidence to suggest longer-range lattice-based exchange.

Complex **8** has a similar essentially isolated 2 × [1 × 3] structure, but has an additional isolated Ni(II) cation in the lattice. The moment per mole (Figure 15) drops from 8.5 μ_B at 300 K to 3.5 μ_B at 2 K, with an overall profile similar to that of **7**, except that the moment at 300 K is somewhat higher, consistent with the presence of an extra Ni(II) center. The magnetic data were fitted to an exchange Hamiltonian
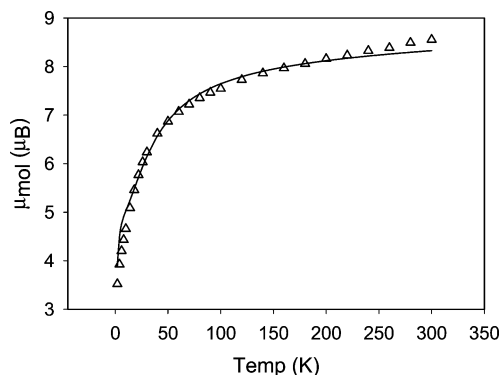
Figure 15. Variable-temperature magnetism for **8** (see text for fitted parameters).

(eq 3), combining two isolated Ni₃ subunits with a single J value as before, but also including an extra term to account for the isolated Curie-like paramagnetic center. The solid line in Figure 15 represents the best fit for $g_{av} = 2.24(2)$, $J = -16(1)$ cm^{-1}, TIP = 1500 × 10^{-6} cm³ mol^{-1}, $\rho = 0.001$, $\theta = -2$ K ($10^2 R = 4.4$).

$$H_{ex} = -J(S_1 S_2 + S_2 S_3 + S_4 S_5 + S_5 S_6) + S_7 \qquad (3)$$

The comparison between **7** and **8** is satisfying in the sense that most derived parameters have comparable values, with the exception of J. Despite comparable Ni−O−Ni angles in the two systems, antiferromagnetic exchange is stronger in **8**. Two significant differences emerge in the structures and properties of **7** and **8**. The central ligand segment has an anti conformation in **7** and a syn conformation in **8**, and the ligands in **7** have a −1 charge overall, whereas those in **8** have a −2 charge. This clearly can be associated with the different exchange effects, and it is reasonable to assume that the ligand charge situation is more important and reflects a more efficient alignment of the Ni d orbitals through the oxygen bridging atoms.

The heptanuclear cobalt complex **9** shows a slight variation in moment from 9.3 μ_B at 300 K to 8.1 μ_B at 2 K (Figure S2, Supporting Information). These values are consistent with the presence of three $S = {}^3/_2$ Co(II) centers in an essentially uncoupled arrangement, in complete agreement with the structure, which shows that the four diamagnetic Co(III) centers are in the grid corner equivalent positions, leading to very long distances between the Co(II) centers.

Compound **10** has a [3 × 3] [Ni₉-(μ-O)₁₂] grid structure (vide supra) and exhibits a magnetic profile (μ_{mol} vs T; Figure 16) typical of a homovalent M₉ [3 × 3] grid, with a moment at 300 K of 9.4 μ_B, dropping smoothly to 3.2 μ_B at 2 K, indicating intramolecular antiferromagnetic exchange. The room-temperature moment is consistent with the presence of nine Ni(II) centers (3.1 μ_B per metal). The value at 2 K
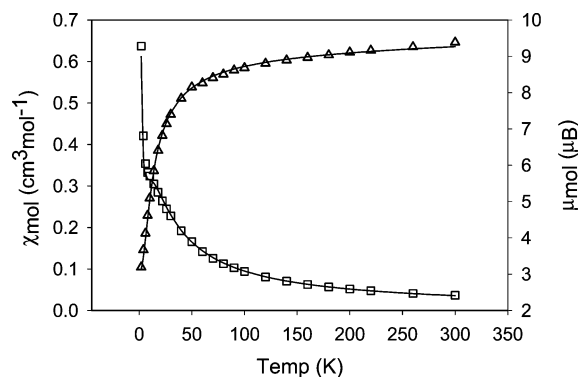
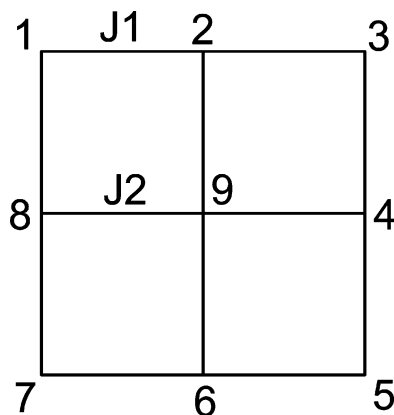**Figure 16.** Variable-temperature magnetism for **10** (see text for fitted parameters).

Figure 17. Magnetic exchange model for [3 × 3] M_9-(μ-O)$_{12}$ grid.

is indicative of the presence of a ground state $S' = {}^2/_2$, expected on the basis of the presence of an odd number of Ni(II) centers in the low-temperature limit. The isotropic, spin-only, exchange Hamiltonian (eq 4) (see Figure 17 for model) should theoretically include two different J values. However, previous analyses with Mn(II)$_9$ grids suggest that $J_1 \approx J_2$, and this approach was employed in the analysis of the magnetic data for **10**.

$$H_{ex} = -J_1\{S_1 \cdot S_2 + S_2 \cdot S_3 + S_3 \cdot S_4 + S_4 \cdot S_5 + S_5 \cdot S_6 + S_6 \cdot S_7 + S_7 \cdot S_8 + S_1 \cdot S_8\} - J_2\{S_2 \cdot S_9 + S_4 \cdot S_9 + S_6 \cdot S_9 + S_8 \cdot S_9\} \quad (4)$$

The total spin state combinations and their energies for this model (eq 1, $J_1 = J_2$) were calculated using normal vector coupling procedures within *MAGMUN,* version 4.1,[42] and the data for **10** fitted accordingly. A very good fit gave $g_{av} = 2.178(6)$, $J_1 = J_2 = -5.3(1)$ cm^{-1}, TIP $= 1750 \times 10^{-6}$ cm^3 mol^{-1}, $\alpha = 0.0001$, and $10^2 R = 1.3$. The solid lines in Figure 16 were calculated with these parameters. This exchange integral is slightly higher than the values

obtained for comparable Mn(II)$_9$ grids, but typical for a μ-O-bridged polynuclear nickel(II) system.

Conclusions

The use of ligand design strategies to produce predetermined coordination arrangements via the self-assembly approach has met with considerable success with the common formation of square [3 × 3] grids with certain metal ions, using tritopic ligands based on 2,6-pyridine dicarboxylic acid hydrazone as the central unit, and in most cases high yields of the nonametallic grids are obtained. The balance of coordination pocket donor characteristics and metal-ion donor and geometric preferences are clearly critical to the reaction outcome, but competition from other ligands (e.g., solvent, coordinating anions) and Lewis acid substitutes (e.g., H$^+$), can lead to completely different products. In the present study we have shown that mononuclear, dinuclear, hexanuclear, heptanuclear, and different nonanuclear complexes can also be synthesized with some tritopic picolinic dihydrazone ligands starting with iron(III), nickel(II), cobalt(II), and copper(II) salts. These products have been identified by the examination of crystalline products and the use of X-ray structural analyses to determine product identity. It clearly points to the fact that oligomers can form in these self-assembly reactions when grid molecules are the ultimate targets. However, in many cases, these oligomers are not implicated directly as intermediates in grid formation, which clearly indicates that a number of different reaction pathways toward product formation are involved. As more examples within this class of complexes are documented, the grid assembly mechanism will hopefully be revealed in more detail.

Supporting Information Available: Figures S1 and S2 in PDF format. This material is available free of charge via the Internet at http://pubs.acs.org. X-ray crystallographic data in CIF format for **1**−**9** have been deposited with the Cambridge Crystallographic Data Center, CCDC Nos. 658405−658413. Copies of this information may be obtained free of charge from The Director, CCDC, 12 Union Road, Cambridge, CB2 1EZ, U.K. (fax +44-1223-336033; e-mail deposit@ccdc.cam.ac.uk; http://www.ccdc.cam.ac.uk).

IC7016787